Robotica (2010) volume 28, pp. 241–252. © Cambridge University Press 2009
doi:10.1017/S0263574709990622

Suturing and tying knots assisted by a surgical robot system in laryngeal MIS

Huijuan Wang†, Shuxin Wang†*, Jienan Ding‡ and Haifeng Luo†

† *School of Mechanical Engineering, Tianjin University, Tianjin 300072, China*
‡*Department of Mechanical Engineering, Columbia University, New York, NY 10027, USA*

(Received in Final Form: October 27, 2009. First published online: December 7, 2009)

SUMMARY

Suturing and tying knots assisted by surgical robot systems are complicated and time-consuming tasks in minimally invasive surgery (MIS). It is almost impossible to perform these operations in laryngeal MIS because motions of the end-effectors are greatly confined by a narrow and long laryngoscope tube. This paper presents the robot-assisted operations of suturing and knot-tying in a laryngeal surgery under a self-retaining laryngoscope, which has a greatly confined workspace. In order to use robot assistance to perform the suturing and knot-tying tasks in such a workspace, an appropriate suturing path is planned. The suturing path planning is completed based on a knot-tying algorithm called the bending-twisting knot-tying (BTKT). A robot system for laryngeal MIS called MicroHand III is designed. The kinematical model of the system is developed in the paper. The simulation and experimental results have shown that suturing and knot-tying assisted by MicroHand III system are successful.

KEYWORDS: Surgical robot; Bending-twisting knot-tying (BTKT); Suturing path planning; Kinematic model.

1. Introduction

Currently, surgical robot systems have been introduced in frontier medical fields for their precise orientation and stability of movement.[1] These advantages facilitate surgeons to effectively carry out a variety of operations in neurological surgery,[2] eye surgery,[3] orthopedic surgery,[4–6] and radiosurgery.[7,8] The application of surgical robot systems in minimally invasive surgery (MIS)[9] provides a new perspective on their development. MIS is an operation of performing surgery through small incisions with endoscopic tools. Compared with open surgery, MIS offers distinct advantages of minimizing invasiveness, including less blood loss and tissue trauma, lower risk of postoperative infection, less pain experienced by the patient, and shorter recovery time. The recently developed robots in master–slave configurations, such as the ZEUS™ Surgical System and the da Vinci® Surgical System, are successful minimally invasive surgical robot systems. These systems have received clearance from the Food and Drug Administration (FDA) to be marketed in the United States.[10,11] Surgical robotic systems facilitate surgeons to effectively carry out a variety of minimally invasive operations including cholecystectomy (removal of the gallbladder),[12,13] cystectomy (removal of the urinary bladder),[14] prostatesectomy (removal of the prostate gland),[15] coronary artery bypass,[16] and mitral valve repair.[17,18] However, although robot-assisted MIS is beneficial to patients, surgeons have to cope with reduced dexterity and perception. In the operation, the instruments used in surgery are usually long and have few degrees of freedom (DoFs). Tactile feedback is lost. Visual feedback is reduced to a two-dimensional image. These factors make suturing and tying knots in robot-assisted MIS complex and time-consuming.[19] Performance of the tasks of suturing and tying knots is one of the most important factors for a surgical robot system.

Compared to thoracic MIS and laparoscopic MIS, in laryngeal MIS, the workspace inside a self-retaining laryngoscope is smaller. McLeod[21] and Hockstein[22] revealed that the self-retaining laryngoscope can provide only limited exposure of the lesion, but greatly restricted the movement of end-effectors. Motions of the instruments are confined severely because these instruments have to deal with the lesions through a long laryngoscope tube. Complex operations, especially suturing and tying knots, are almost impossible to be accomplished with current surgical robot systems. In 2005, the da Vinci system assisted surgeons in performing a procedure in the neck of a patient.[20] The end-effectors of the system could not approach the right place in time. The tasks of suturing and tying knots could not be performed due to the too large mechanisms of the robot system compared to the small workspace. Additionally, it took a long time for surgeons to prepare for the operating procedure and therefore reduced the efficiency of the operation. The research group at Tianjin University in China developed a robot system (called MicroHand II) for laryngeal surgery.[23] The system contains a series of end-effectors with diameters of only 3 mm. The system can perform coordinated motions of two end-effectors inside a laryngoscope tube and accomplish tasks such as cutting and dissection. However, the tasks of suturing and tying knots still cannot be executed by MicroHand II because the end-effectors have only two DoFs (rotating and open–close). The

* Corresponding author. E-mail: shuxinw@tju.edu.cn

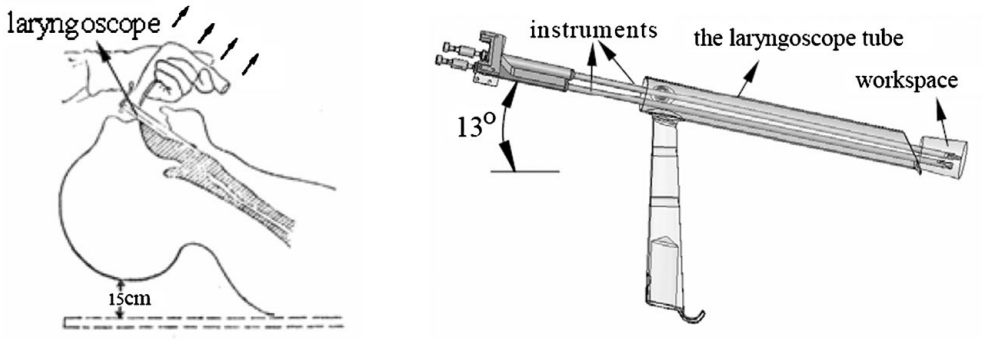

1*a*. Laryngeal MIS with a self-retaining laryngoscope 1*b*. Two end-effectors of a surgery robot system inside a laryngoscope

Fig. 1. Laryngeal MIS with a laryngoscope.

research group at Johns Hopkins University developed a snake robot system.[24] It is featured by end-effectors that have multiple DoFs with a diameter of 4 mm. The system can assist surgeons to accomplish the tasks of suturing and tying knots in a small workspace. However, the mechanisms of the system are very complex, and the end-effectors of the system can provide only a maximum grasping force of 1 N.

Contributions to the development of suturing and knot-tying have been made on modeling of sutures, needles and tissues,[25–27] analysis of knot-tying motion and path planning for stitching and knot-tying,[26,28,29] development of new methods for tying knots,[1,30,31] and investigation of mechanisms of suturing and tying knots.[32,33] Pai[25] proposed a linear object deformation model using the Cosserat formulation for tying knots. This suture model could deal with rotational and translational displacements, including flexure, torsion, and extension of a linear object. Phillips[27] used a particle-based model of a rope to simulate knot-tying problems. However, the suturing operation was not taken into consideration in these literatures. Brown[26] brought forward a kinematic scheme "follow the leader" to plan the path of suturing and knot-tying. With this method, a virtual rope was simulated in real time without bending and twisting. Saha[28] presented motion planning for robotic manipulation of deformable linear objects without considering the operations of suturing and knot-tying. Nageotte[29] just focused on the kinematics analysis of the stitching task and presented a method for needle trajectories to minimize the deformation of the tissues during the task but did not present tying knots. Wang[1] proposed a novel approach to knot-tying in a small workspace for surgical robot systems. Kang[30] presented an autonomous suturing algorithm but the algorithm depended on the special robot system EndoBot. Automated knot-tying in MIS was presented by Kuniholm,[31] but this algorithm was only for fixation in a cardiovascular procedure. Murphy[32] introduced 12 ways to create a square knot that can be applied in endoscopic surgery with second-generation purpose-designed instruments. Some instruments were designed for surgical suturing and tying knots such as the instrument designed by Ustuner[33]. These contributions promote the development of surgical robot systems. However, there are few open literatures that report the research on suturing and tying knots in a small, confined workspace.

This paper aims at finding out an approach to suturing and knot-tying in a confined workspace, particularly in robot-assisted laryngeal MIS. The paper is divided into seven sections as follows. The workspace in laryngeal MIS is analyzed in Section 2. Section 3 proposes a path planning for the suturing operation and the bending-twisting knot-tying (BTKT) method for tying knots. The general design of the MicroHand III robot system is introduced in Section 4. Section 5 presents the geometric and kinematic models of suturing and knot-tying tasks. The suturing simulations and MicroHand III-assisted experiments are presented in Section 6. Finally, conclusions are presented at the end of the paper.

2. Workspace of Laryngeal MIS

A self-retaining laryngoscope is one of the frequently used tools in laryngeal MIS. Through a long laryngoscope tube the surgeon masters surgery instruments to touch and dissect the lesions inside the larynx, as shown in Fig. 1a. So the workspace in laryngeal MIS is greatly confined by the sizes of the laryngoscope used. The laryngoscope tube usually has two ends. The one closer to the surgeon in an operation can be defined as the near-end while the opposite end is the far-end. The shape of the near-end is approximately a circle with a diameter of 25–30 mm. The shape of the far-end is usually a circle with a diameter of 15–20 mm. The length of laryngoscope tubes ranges from 150 to 180 mm[34]. The model of the laryngoscope chosen in our research is shown in Fig. 1b. The laryngoscope tube is 175 mm long and its near-end and far-end are circles with a diameter of 30 mm and 20 mm respectively, as shown in Fig. 2.

According to the sizes of the laryngoscope and the operating requirements of laryngeal MIS, the whole space in laryngeal surgery can be divided into three subspaces: the space between the far-end and the lesion, the basic operating space, and the reachable space, as shown in Fig. 2. The distance between the far-end and the lesion is usually 5–10 mm, and so the space between the far-end and the lesion in this research is a cylindrical area of Φ20 mm × 5–10 mm. The radial size of the basic operating space is usually a bit

https://doi.org/10.1017/S0263574709990622 Published online by Cambridge University Press

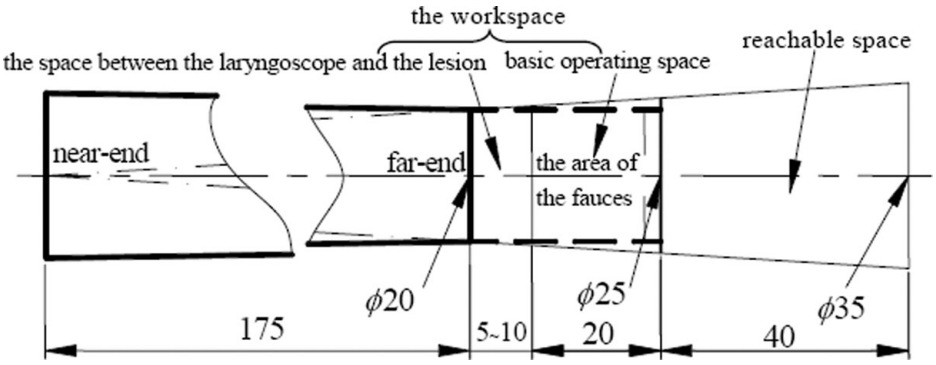

Fig. 2. The operating space in a laryngeal surgery with a self-retaining laryngoscope.

more than the diameter of the far-end which is usually Φ15–20 mm. So the radial size of the basic operating space can be defined as Φ20–25 mm. The maximum axial size of the basic operating space depends on the length of the lesion area. When the lesion occurs at both arytenoid cartilages (or laryngeal chamber and vocal ligaments, which are all in the area of the fauces, shown in Fig. 2), the lesion area is 20 mm long. So the basic operating space is a cylindrical area of Φ20–25 mm × 20 mm. The reachable space is defined as the area where the instruments confined by a long laryngoscope tube can approach. The reachable space in this research is a conical area of Φ25 mm × Φ35 mm × 40 mm, as shown in Fig. 2. The workspace inside the laryngoscope is usually defined by the sum of the basic operating space and the space between the laryngoscope and the lesion, as shown in Fig. 2.

In laryngeal MIS, an instrument should have at least six DoFs in order to perform a procedure[35]. The instrument can thus rotate and translate inside the laryngoscope tube, as shown in Fig. 3. However, the scopes of the movements of the instrument are greatly confined. The translating movements should be within the workspace mentioned above. In order to describe the scope of the orientation of the instrument in laryngeal MIS, a local coordinate frame is established, which is illustrated in Fig. 3. The origin o is assumed at the center of the near-end. And the variables of the instrument rotating about the axes of the frame z, x, and y are denoted by θ_z, λ_x, and λ_y respectively.

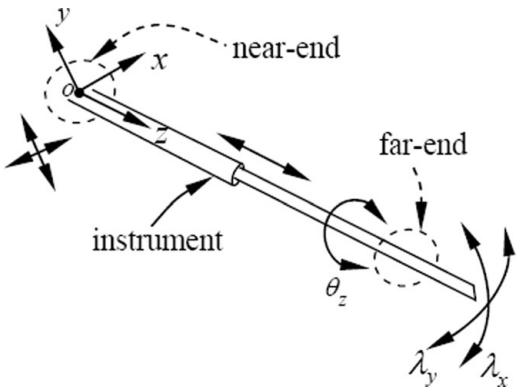

Fig. 3. Six DoFs of an instrument confined by a laryngoscope tube.

p coincides with the origin o. The instrument should move within a right circular cone with a highness of 175 mm, which is the length of the laryngoscope, and a radius of 10 mm, which is the radius of the far-end. When $0 < \rho_p \leq 10$ mm, the instrument should move within a cone of $\Phi 2\rho_p$ mm × Φ20 mm × 175 mm. If the point p is fixed at a point in the near-end plane, the instrument should move within an oblique circular cone. When 10 mm $< \rho_p \leq 12.5$ mm, the configurations of the instrument are similar to those that occur with $0 < \rho_p \leq 10$ mm. Due to the symmetry of the plane of xoy, the variable λ_y has the same range as the variable λ_x. So the orientation of the instrument confined by the tube can be obtained by the following equations:

$$\begin{cases} 0 \leq \theta_z \leq 2n\pi, n \in N, n \geq 1 & \\ -0.0571 \leq \lambda_x, \lambda_y \leq 0.0571 & \text{when } \rho_p = 0 \\ \arctan((10-\rho_p)/175) \leq \lambda_x, \lambda_y \leq \arctan((10+\rho_p)/175) \quad \text{or} & \text{when } 0 < \rho_p \leq 10\,\text{mm} \\ -\arctan((10+\rho_p)/175) \leq \lambda_x, \lambda_y \leq -\arctan((10-\rho_p)/175) & \\ \arctan((\rho_p-10)/175) \leq \lambda_x, \lambda_y \leq \arctan((\rho_p+10)/175) \quad \text{or} & \text{when } 10\,\text{mm} < \rho_p \leq 12.5\,\text{mm} \\ -\arctan((\rho_p+10)/175) \leq \lambda_x, \lambda_y \leq -\arctan((\rho_p-10)/175) & \end{cases} . \tag{1}$$

It should be that $0 \leq \theta_z \leq 2n\pi$, $n \in N, n \geq 1$, and the variables λ_x and λ_y have the same ranges due to the symmetry in the xoy plane. The cylindrical coordinate system is used in this work to describe the orientations of the instruments. The crossing point of the center line of an instrument and the plane of the near-end is denoted by p and the distance between the points p and o is denoted by ρ_p. Then there are three conditions to be discussed. When $\rho_p = 0$, the point

In general, the orientational variables of an instrument λ_x and λ_y have the same range in radian [−0.12787, 0.12787]. Transferring the radians into degrees, it is obtained that both λ_x and λ_y are in the range of [−7.3264°, 7.3264°]. The projections of an instrument inside a laryngoscope tube and the far-end of the tube into the plane of the near-end can illustrate explicitly the position and the orientation of the instrument, which are shown in Fig. 4.

https://doi.org/10.1017/S0263574709990622 Published online by Cambridge University Press

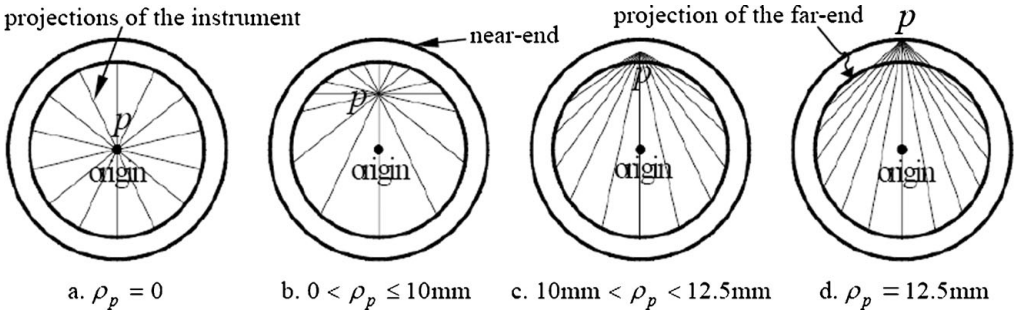

Fig. 4. The projections of an instrument and the far-end into the near-end plane.

3. Analysis of Suturing and Tying Knots for Robot-assisted Laryngeal MIS

Cao[36] and Kang[37] both introduced motion analysis of the task of tying a simple knot in a surgical procedure. The process of tying a knot can be divided into four subtasks: stitching in the right place, forming loops, tying a surgical knot, and securing the knot. The final step involves the proper placement of the knot and the tightening of the knot with a specified tension.

The first subtask, stitching, involves tying a simple knot and is also called the task of suturing. The motion of a single stitch in surgery can be divided into the following three steps: (1) positioning the entry point and the exit point (the distance from the entry point to the edge of the wound, as well as the distance from the edge to the exit point, should be approximately equal to the thickness of the tissue being sutured); (2) grasping the needle and inserting it at right angles into the tissue; (3) passing through both aspects of the suture line and exiting at right angles with a proper path (it should not drag the needle through the tissue but follow the curve of the needle).

If the end-effectors of a surgical system have enough DoFs and the workspace is large enough, a robot system can execute the tasks of suturing and tying knots with any method.[19,30] However, in laryngeal MIS under a self-retaining laryngoscope, the motions of the end-effectors are greatly confined by the laryngoscope tube. The motion of tying knots cannot be completed by end-effectors using conventional knot-tying methods, which require a large workspace.[1] In this paper, the knot-tying process is completed by an improved BTKT method.[1] The operation is shown in detail in Fig. 5 and is described as follows:

(a) Position the entry point and the exit point, grasp the needle, and insert it at right angles into the tissue. Pull out the suture and leave two suture tails with an equal length. Place the two end-effectors parallel to each other inside the laryngoscope tube, and grasp the two tails separately along the tangent to the grasp points.
(b) Rotate Tool 1 clockwise (looking from the near-end of the laryngoscope tube) to form a loop on Thread 1 using the BTKT method.
(c) Open Tool 2 to loosen Thread 2 and move Tool 2 over the loop.
(d) Bend the jaws of Tool 2 and grasp Thread 2 through the loop.
(e) Pull out Thread 2 through the loop and form a knot.
(f) Grasp the two tails, cross the two tools with Tool 2 above, and move the tools in opposite directions so that the two grasping points are away from each other. Therefore, the configuration of a simple knot is adjusted.
(g) Change the grasping angles between the end-effectors and tails. Let Tool 1 steadily grasp Thread 1 along the normal line to the grasping point and let Tool 2 steadily grasp Thread 2 along the normal line to the grasping point.
(h) Rotate Tool 1 and Tool 2 respectively with the same velocity and move the end-effectors appropriately to the wound until the knot is tightened at the right place. The same velocity of the tools can ensure that the amounts of thread wrapped around the tools are equal.

4. The Laryngeal Surgical Robot System MicroHand III

A compact and light laryngeal surgical robot system, MicroHand III is designed according to the requirements of suturing and knot-tying operations in laryngeal MIS, as illustrated in Fig. 6. The system is designed with a modular method and is composed of three configurations: the passive bracket, the active manipulator, and the end-effectors.

The passive bracket has six DoFs in the spatial dimension. It can move to any position with any posture in its reachable space with a size of 200 mm × 200 mm × 100 mm. The bracket has a locking mechanism that can easily fix the bracket at any position. The movements of the bracket are independent from the operations of the active manipulator or end-effectors. The bracket has gravity compensation devices that enable surgeons to move the bracket easily.

The active manipulator is fixed on the passive bracket and above the face of the patients. Such a setup is arranged for safety. The active manipulator has two prismatic DoFs and three revolute DoFs. The prismatic DoFs are realized by a high precision screw slider mechanism driven by motors. Two of the revolute DoFs are realized by a parallelogram linkage and the other revolute DoF is realized by gear trains. The workspace of the active manipulator is 20 mm × 20 mm × 20 mm.

The end-effectors have a diameter of 4 mm and a weight of less than 100 g. They are equipped with two jaws similar to

https://doi.org/10.1017/S0263574709990622 Published online by Cambridge University Press

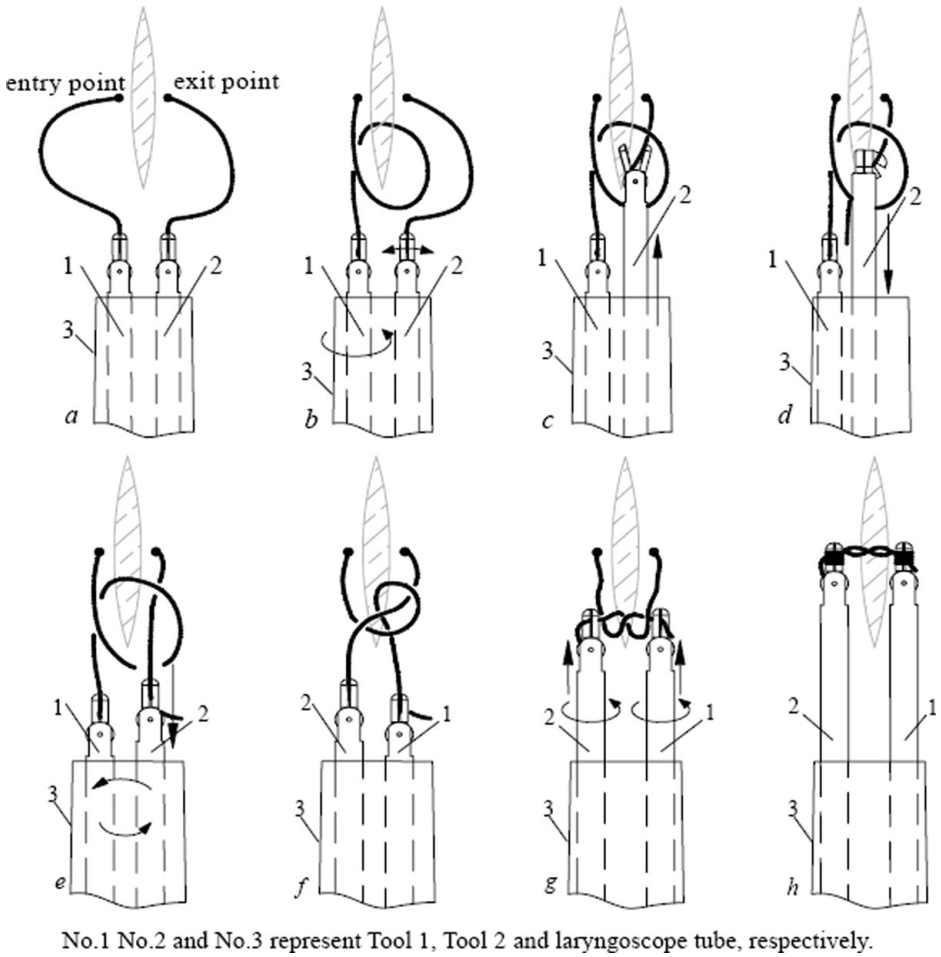

Fig. 5. Bending-twisting knot-tying algorithm.

forceps and needle holders to accomplish complex operations such as suturing and tying knots. The grasping force is about 4 N[35]. The end-effectors also have an extra rotating joint to ensure the bending behavior. Therefore, the end-effectors have three independent DoFs, rotating, bending, and open–close. The bending DoF facilitates the end-effectors to deal with the lesion with a required gesture. The end-effectors can be actuated to reach any position in the workspace of Φ20 mm × Φ25 mm × 20–30 mm. The gesture can be maintained during the moving process. The gesture angles of the end-effectors range from −10° to 10°. Each end-effector has a quick interchangeable unit that can be quickly interchanged during surgical procedures.

The dexterity of end-effectors has a vital influence on the performance of the whole system. The end-effectors have to be small and long enough to work inside the long

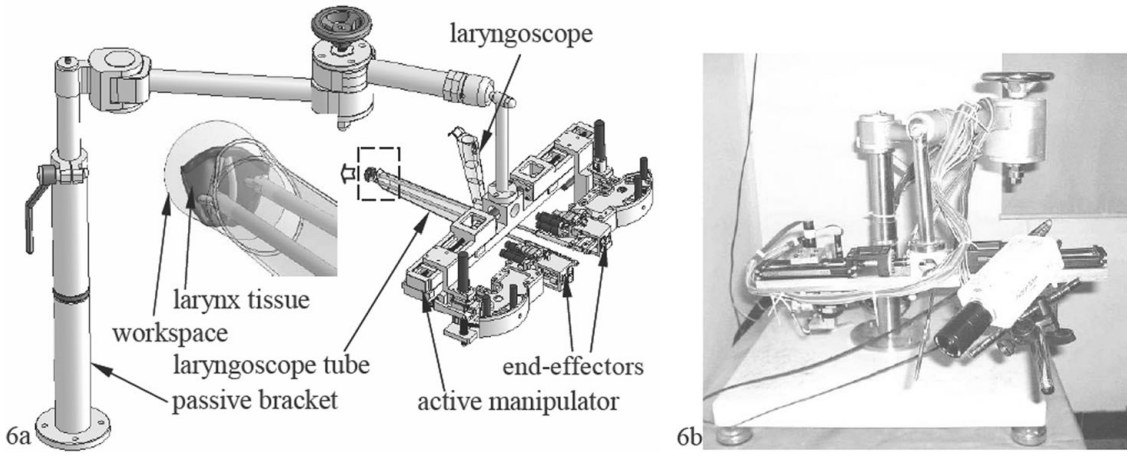

Fig. 6. The laryngeal surgical robot system: MicroHand III.

https://doi.org/10.1017/S0263574709990622 Published online by Cambridge University Press

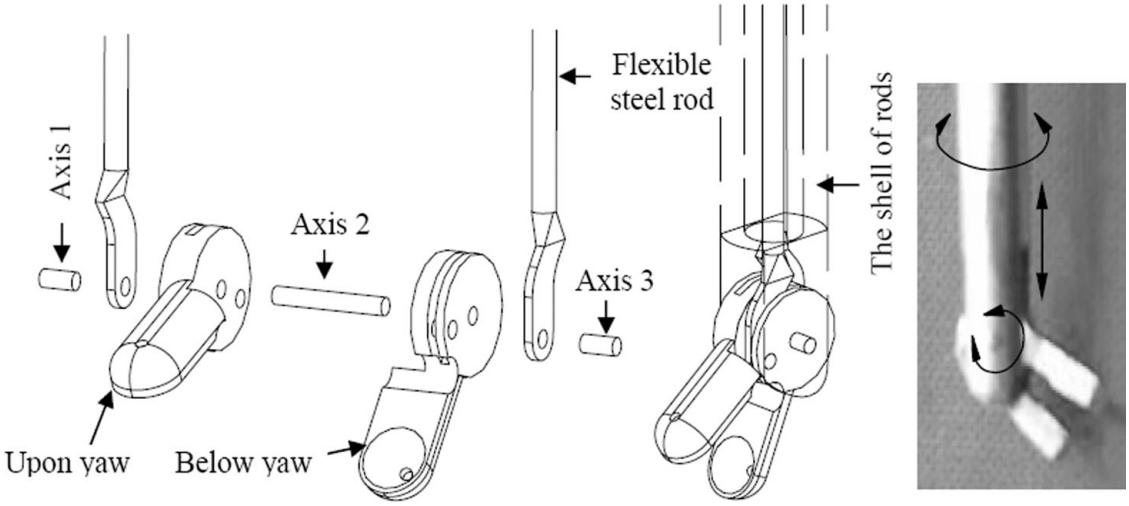

Fig. 7. The end-effector of MicroHand III.

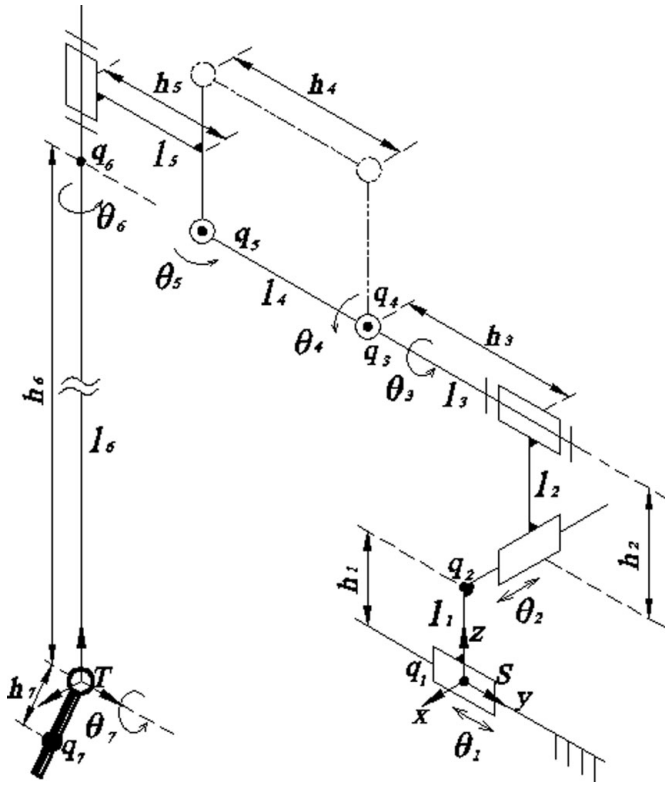

Fig. 8. The kinematic model of the MicroHand III system.

laryngoscope tube cooperatively and avoid collision in the small confined workspace. The components of the end-effectors of the MicroHand III are shown in Fig. 7.

5. Mathematical Model of Suturing and Tying Knots with MicroHand III

The kinematic models of MicroHand III for performing the suturing and knot-tying operations in simulation and experiments are established in this section.

5.1. The kinematic model of MicroHand III

The kinematic model of the MicroHand III system is modeled on screws theory,[38,39,40] as shown in Fig. 8. The passive bracket of the MicroHand III system is always fixed during the operation after being adjusted to an appropriate position. Therefore, it is viewed as a part of the base spatial coordinate frame of the whole system.

During the operations of suturing and tying knots, the grasping point on end-effectors is consistent with the position of $\boldsymbol{q}_7$. Considering the bending joint of the end-effectors, the joints of the system are numbered from 1 to 7, as shown in Fig. 8. There are two prismatic and five revolute DoFs. The links are numbered accordingly so that joint i connects links $i-1$ and i. Link 0 is the part fixed on the passive bracket and link 6 is attached rigidly to the end-effector. Link 7 is attached rigidly to one jaw of the end-effector. Prismatic joints are described by a linear displacement $\theta_i \in \Re$ along the axis shown in Fig. 8, and positive displacement is along the direction of the axis.

For revolute joints, the joint variables are given by an angle $\theta_i \in [0, 2\pi)$ and $\theta_i \in S^1$, where S^1 is denoted as a unit circle in the plane. An angle is positive if it represents a clockwise rotation along the direction of the axis shown in Fig. 8. The joint space of the system including the bending joint of the end-effectors is denoted as Q, and $Q = T^5 \times \Re^2$, where $T^p = S^1 \times \cdots \times S^1$, $p = 5$.

The overall kinematics of the system in the spatial coordinate frame o–xyz with screw representation[35] is represented by the mapping $g_{st} : Q \to SE(3)$, and given by

$$g_{st}(\boldsymbol{\theta}) = \mathrm{e}^{\hat{\xi}_1\theta_1} \cdots \mathrm{e}^{\hat{\xi}_7\theta_7} g_{st}(0), \tag{2}$$

where $\xi_i = \begin{bmatrix} \mathbf{v}_i \\ \boldsymbol{\omega}_i \end{bmatrix}$. $\boldsymbol{\omega}_i$ is the unit vector of the axis of a revolute joint i. $v_i = -\boldsymbol{\omega}_i \times \boldsymbol{q}_i = \hat{\boldsymbol{\omega}}_i \cdot \boldsymbol{q}_i$, and $\boldsymbol{q}_i$ is a point on the axis of joint i. For a prismatic joint i, $\boldsymbol{\omega}_i = 0$. $\hat{\xi}_i = \xi_i^{\wedge} = \begin{bmatrix} \mathbf{v}_i \\ \boldsymbol{\omega}_i \end{bmatrix}^{\wedge} = \begin{bmatrix} \hat{\boldsymbol{\omega}}_i & \mathbf{v}_i \\ 0 & 0 \end{bmatrix}$, where $\hat{\boldsymbol{\omega}}_i = \boldsymbol{\omega}_i \times$. $g_{st}(0)$ is the configuration of the Grasping point $\boldsymbol{q}_i$ when all the joint variables are 0, and

$$g_{st}(0) = \begin{bmatrix} & & 0 \\ I & & -h_3 - h_4 - h_5 \\ & & h_1 + h_2 - h_6 - h_7 \\ 0 & & 1 \end{bmatrix}.$$

https://doi.org/10.1017/S0263574709990622 Published online by Cambridge University Press

Table I. Screws of joints of the system.

Ji	ω_i	q_i	$\mathbf{v}_i$
1	–	$[0\ 0\ 0]^T$	$[0\ 1\ 0]^T$
2	–	$[0\ 0\ h_1]^T$	$[1\ 0\ 0]^T$
3	$[0\ 1\ 0]^T$	$[0\ -h_3\ \ h_1+h_2]^T$	$[-(h_1+h_2)\ 0\ 0]^T$
4	$[1\ 0\ 0]^T$	$[0\ -h_3\ \ h_1+h_2]^T$	$[0\ (h_1+h_2)\ h_3]^T$
5	$[1\ 0\ 0]^T$	$[0\ -h_3-h_4\ \ h_1+h_2]^T$	$[0\ (h_1+h_2)\ h_3+h_4]^T$
6	$[0\ 0\ 1]^T$	$[0\ -h_3-h_4-h_5\ \ h_1+h_2]^T$	$[-(h_3+h_4+h_5)\ 0\ 0]^T$
7	$[0\ 1\ 0]^T$	$[0\ -h_3-h_4-h_5\ \ h_1+h_2-h_6-h_7]^T$	$[h_6+h_7-(h_1+h_2)\ 0\ 0]^T$

Table II. Ranges of joint variables.

θ_i	θ_1	θ_2	θ_3	θ_4	θ_5	θ_6	θ_7
Scopes	±20 mm	±18 mm	±5°	±8.5°	±5°	±180°	±90°

The parameters of screws of the system are illustrated in Table I. The ranges of the joint variables are shown in Table II.

The inverse kinematics problem of the MicroHand III system must be solved to complete the tasks of suturing and knot-tying through a narrow and long laryngoscope tube. We choose the minimum joint velocity that gives the desired workspace velocity since the system is kinematically redundant. The relationship between joint velocity $\dot{\boldsymbol{\theta}}$ and the velocity of point $\boldsymbol{q}_7$, $V_{st}^{q_7}$ is

$$\dot{\boldsymbol{\theta}} = J_{st}^{+}(\boldsymbol{\theta}) V_{st}^{q_7}, \tag{3}$$

where $J_{st}^{+}(\boldsymbol{\theta}) = (J_{st}^{s}(\boldsymbol{\theta}))^T \cdot (J_{st}^{s}(\boldsymbol{\theta}) \cdot (J_{st}^{s}(\boldsymbol{\theta}))^T)^{-1}$ is the Moore–Penrose generalized inverse of the spatial Jacobian of the system $J_{st}^{s}(\boldsymbol{\theta})$. It should be $J_{st}^{s}(\boldsymbol{\theta}) = [\,\xi_1 \quad \xi_2' \quad \cdots \quad \xi_7'\,]$. And

$$\xi_i' = \left(\frac{\partial g_{st}(\boldsymbol{\theta})}{\partial \theta_i} g_{st}^{-1}(\boldsymbol{\theta}) \right)^{\vee}, i = 2, \ldots, 7,$$

as introduced by Murray[40].

After the suturing path and knot-tying algorithm are established, the configurations of $\boldsymbol{q}_7$ can be achieved by $g(t) \in SE(3)$. The spatial velocity $\hat{V}_{st}^{q_7} = \dot{g} g^{-1}$ can be calculated. And then $V_{st}^{q_7} = (\hat{V}_{st}^{q_7})^{\vee}$ is known. The joint variables $\boldsymbol{\theta}$ can be obtained after the ordinary differential equation (3) is solved. With the known joint variables, the control system can actuate the whole system and complete the tasks.

5.2. Mathematical description of suturing operation

An 8-mm 3/8 needle that is formed in an arc of 3/8 of a circle with a diameter of 8 mm is chosen to perform the operation of stitching.

In the quantitative analysis of the motion of a single stitch, two rules have to be followed. First, the path of suturing should be an arc that follows the curve of the needle. The path is written by $\|\boldsymbol{p} - \boldsymbol{p}_c\| = r$, where $\boldsymbol{p}$ and $\boldsymbol{p}_c$ are respectively the tip of the needle and the center of the path, and r is the

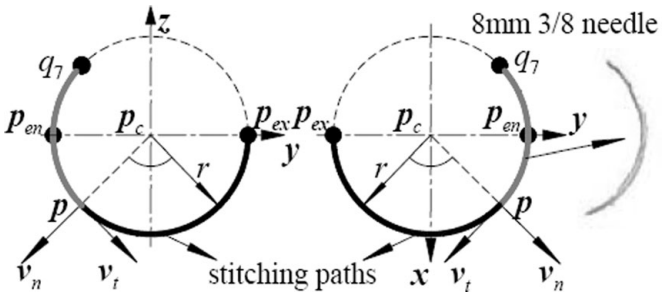

Fig. 9. Path planning of a stitch.

radius of the path and $r = 8$ mm. Point $\boldsymbol{p}_c$ is a fixed point in the spatial coordinate frame o–xyz since it is associated with the wound and tissues according to surgical suturing techniques. Secondly, the velocity of stitching the tissues should be even in order to maintain the correct tension along the wound. So the instantaneous velocity of $\boldsymbol{p}$ should be along the tangent to the path of the stitch and its absolute quantity denoted by v should be constant, while its velocity along the normal is zero. In Fig. 9, Let $\boldsymbol{p}_{en}$ and $\boldsymbol{p}_{ex}$ be the positions of the entry point and the exit point respectively. And $\boldsymbol{v}_t$ denotes the velocity along the tangent to the path and $\boldsymbol{v}_n$ is the velocity along the normal direction. So $\boldsymbol{v}_t = \boldsymbol{v}$ and $\boldsymbol{v}_n = 0$.

The path of point $\boldsymbol{q}_7$ is the same as the path of $\boldsymbol{p}$ with a delay time of $3\pi r/8v$ due to the length of the needle. We just operate the stitching motion in the vertical (yz) and horizontal (xy) planes. Assume that the stitching direction in the xy plane is negative, and the stitching in the yz plane is along the positive direction, as shown in Fig. 9. The path of q_7 for the stitching task in the yz plane can be obtained by

$$\boldsymbol{q}_{yz}(t) = \boldsymbol{p}_c + \left(0 - r\cos\left(\frac{v}{r}\left(t - \frac{3\pi r}{8v}\right)\right) - r\sin\left(\frac{v}{r}\left(t - \frac{3\pi r}{8v}\right)\right)\right)^{\mathrm{T}}. \tag{4}$$

Also, the path of q_7 for the system stitching in the xy plane can be achieved by

$$\boldsymbol{q}_{xy}(t) = \boldsymbol{p}_c + \left(r\sin\left(\frac{v}{r}\left(t - \frac{3\pi r}{8v}\right)\right) \times r\cos\left(\frac{v}{r}\left(t - \frac{3\pi r}{8v}\right)\right) 0\right)^{T} \tag{5}$$

https://doi.org/10.1017/S0263574709990622 Published online by Cambridge University Press

and the orientation matrices of q_7 during the stitching operation in the yz and xy planes are denoted as $\boldsymbol{R}_{yz}$ and $\boldsymbol{R}_{xy}$ respectively.

$$\boldsymbol{R}_{yz} = \begin{bmatrix} 1 & 0 & 0 \\ 0 & \cos\left(\frac{v}{r}\left(t - \frac{3\pi r}{8v}\right)\right) & -\sin\left(\frac{v}{r}\left(t - \frac{3\pi r}{8v}\right)\right) \\ 0 & \sin\left(\frac{v}{r}\left(t - \frac{3\pi r}{8v}\right)\right) & \cos\left(\frac{v}{r}\left(t - \frac{3\pi r}{8v}\right)\right) \end{bmatrix}$$

and

$$\boldsymbol{R}_{xy} = \begin{bmatrix} \cos\left(\frac{v}{r}\left(t - \frac{3\pi r}{8v}\right)\right) & \sin\left(\frac{v}{r}\left(t - \frac{3\pi r}{8v}\right)\right) & 0 \\ -\sin\left(\frac{v}{r}\left(t - \frac{3\pi r}{8v}\right)\right) & \cos\left(\frac{v}{r}\left(t - \frac{3\pi r}{8v}\right)\right) & 0 \\ 0 & 0 & 1 \end{bmatrix}.$$

Hence, the configurations of $\boldsymbol{q}_7$ can be obtained. For the stitching task in the yz plane,

$$\boldsymbol{g}_{yz}(t) \in SE(3),\ \boldsymbol{g}_{yz}(t) = \begin{bmatrix} \boldsymbol{R}_{yz} & \boldsymbol{q}_{yz}(t) \\ 0 & 1 \end{bmatrix}. \tag{6}$$

And for the system stitching in the xy plane,

$$g_{xy}(t) \in SE(3),\ g_{xy}(t) = \begin{bmatrix} \boldsymbol{R}_{xy} & \boldsymbol{q}_{xy}(t) \\ 0 & 1 \end{bmatrix}. \tag{7}$$

The spatial velocity $\hat{V}_{st}^{q_7}$ is calculated respectively for stitching in yz and xy planes.

$$\hat{V}_{yz}^{q_7} = \dot{\boldsymbol{g}}_{yz}\boldsymbol{g}_{yz}^{-1}, \tag{8}$$

$$\hat{V}_{xy}^{q_7} = \dot{\boldsymbol{g}}_{xy}\boldsymbol{g}_{xy}^{-1}. \tag{9}$$

The ordinary differential equation (3) can be solved after the Eqs. (8) and (9) are calculated. And then the joint variables $\boldsymbol{\theta}$ are obtained for the stitching operation in the yz and xy planes respectively.

5.3. *Mathematical description of tying knots*

The representations of the knot-tying algorithm are shown in Fig. 10. Define ζ_0 as the distance between the entry point and the exit point, $\boldsymbol{\zeta}_0 = \|\boldsymbol{p}_{\text{ex}} - \boldsymbol{p}_{\text{en}}\|$. Tool 1 grasps Thread 1 at $\boldsymbol{q}_7^1$. Tool 2 grasps Thread 2 at $\boldsymbol{q}_7^2$. The effective length of Thread 1 is defined as $L_1(t)$ and the effective length of Thread 2 is defined as $L_2(t)$. Define $\boldsymbol{\zeta}_1 = (\boldsymbol{q}_7^1 - \boldsymbol{p}_{\text{en}})$ and $\boldsymbol{\zeta}_2 = (\boldsymbol{q}_7^2 - \boldsymbol{p}_{\text{ex}})$. $\dot{\boldsymbol{q}}_7^1$ and $\dot{\boldsymbol{q}}_7^2$ are respectively the velocity vectors of the grasping points. $\dot{L}_1$ and $\dot{L}_2$ are respectively the rates of change of the lengths of Thread 1 and Thread 2. To keep track of the thread lengths, the relationship between $\dot{L}_i$ and $\dot{\boldsymbol{q}}_7^i$ $(i = 1, 2)$ must be clarified.

Before a knot is tightened, the tools grasp two threads along the tangents to the grasping points on the threads respectively, as shown in Fig. 10a. If $\dot{\boldsymbol{q}}_7^i$ and $\boldsymbol{\zeta}_i$ form an obtuse angle[30] $(\dot{\boldsymbol{q}}_7^i \cdot \boldsymbol{\zeta}_i < 0)$, then Thread i is not in tension along the tangent, but in torsion caused by the rotation of Tool i which grasps

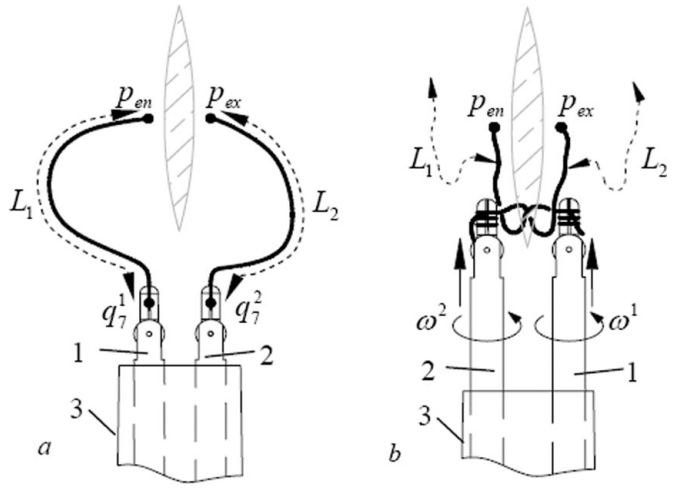

Fig. 10. Representations of the knot-tying algorithm.

the thread. On the contrary, if $\dot{\boldsymbol{q}}_7^i$ and $\boldsymbol{\zeta}_i$ form an acute angle $(\dot{\boldsymbol{q}}_7^i \cdot \boldsymbol{\zeta}_i > 0)$, it is necessary to consider two possibilities. If $\|\boldsymbol{\zeta}_i\| \geq L_i$, then Thread i would be in tension along its tangent; otherwise, $\dot{L}_i = 0$. The rates of change for thread lengths before the tightening of a knot can be summarized as follows:

$$\dot{L}_i(t) = \begin{cases} 0 & \text{if } \dot{\boldsymbol{q}}_7^i(t) \cdot \boldsymbol{\zeta}_i(t) \leq 0 \text{ or } \|\boldsymbol{\zeta}_i(t)\| < L_i(t) \\ \dot{\boldsymbol{q}}_7^i(t)\boldsymbol{\zeta}_i(t) & \text{if } \dot{\boldsymbol{q}}_7^i(t) \cdot \boldsymbol{\zeta}_i(t) > 0 \end{cases} \quad (i = 1, 2). \tag{10}$$

When the knot is being tightened, the tools grasp the threads along the normal lines to the grasping points respectively. When the tools rotate, the threads wrap around the axes of the tools separately, as shown in Fig. 10b. The knot is tightened with the effective lengths of the threads reduced. With this method for tightening the knot, it is satisfied that $\dot{\boldsymbol{q}}_7^i\boldsymbol{\zeta}_i \leq 0$ and $\dot{L}_i \neq 0$. The velocities of tool rotation are respectively defined as ω^1 and ω^2. It is assumed that a cylinder with a diameter of r^i is formed when the tool closes its two jaws. The rate of change for thread length is represented as follows:

$$\dot{L}_i(t) = \dot{\boldsymbol{q}}_7^i(t) \cdot \boldsymbol{\zeta}_i(t) - \omega^i(t)r^i \ (i = 1, 2). \tag{11}$$

When $L_i(t) = \zeta_0$(i = 1,2), the knot-tightening is finished. During this process, $\dot{L}_1(t) = \dot{L}_2(t)$ should be satisfied to ensure that the knot is tied firmly.

6. Simulation and Experiments

Simulation and experiments with the laryngeal robot system MicroHand III are presented in this section.

6.1. *Suturing simulation and experiments*

The simulations of suturing in vertical and horizontal planes are performed respectively with an 8-mm 3/8 needle. Before simulation, the different fixed points $\boldsymbol{p}_c$ for suturing in vertical (yz) and horizontal (xy) planes have been known. So the stitching paths can be achieved with Eqs. (4) and

https://doi.org/10.1017/S0263574709990622 Published online by Cambridge University Press

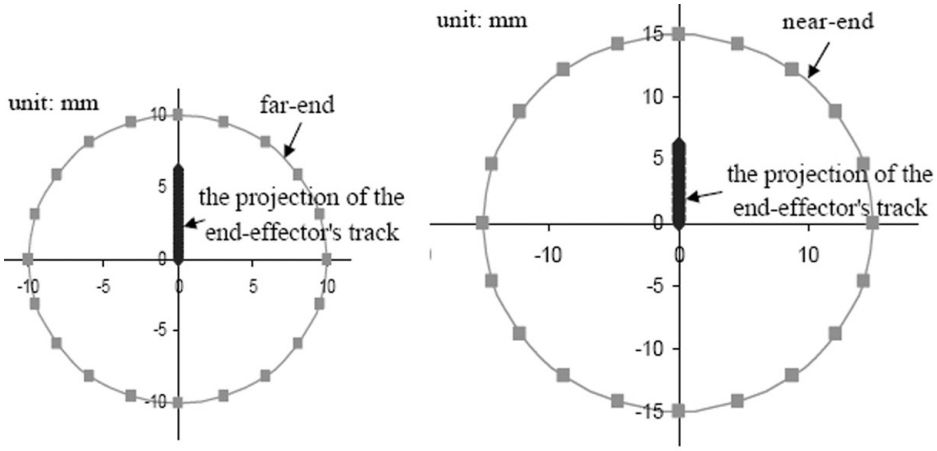

11a. The projection in the far-end 11b. The projection in the near-end

Fig. 11. Simulation of stitching motion in vertical plane under a laryngoscope tube.

(5), respectively. Also, the configuration of $\boldsymbol{q}_7$, $g(t)$, can be obtained by Eqs. (6) and (7). The joint variables $\boldsymbol{\theta}$ of the robot system for suturing in vertical and horizontal planes can be solved with Eqs. (3), (8), and (9). With these $\boldsymbol{\theta}$ and the robot model using the Simulink Toolbox of Matlab, the motions of stitching in vertical and horizontal planes are simulated.

The projections of the tip of the needle onto the far-end and the near-end in vertical simulation are respectively shown in Figs. 11a and 11b. The needle tip projections in horizontal simulation are presented in Figs. 12a and 12b. During the stitching operation, the projections of the needle are inside the far-end and the near-end. The simulation results indicate that it is feasible and dexterous for the system to be moved limitedly and that the MicroHand III system can facilitate surgeons to suture wounds with its end-effectors through the narrow and long laryngoscope tube.

Applying the calculated joint variables $\boldsymbol{\theta}$, the corresponding suturing experiments assisted by MicroHand III in vertical and horizontal planes are also performed with an 8-mm 3/8 needle. The pictures of the needle during the stitching motion in vertical and horizontal planes are shown in Figs. 13 and 14 respectively.

6.2. *Experiments of tying knots*

The BTKT simulation is presented in Ref. 1. And the experiments associated with the BTKT algorithm are assisted by the MicroHand III system, as shown in Fig. 15. Simple knots can be tied effectively via this algorithm. Square knots and surgeon's knots that are composed of simple knots should be tied with this algorithm. The BTKT algorithm is feasible and practical in laryngeal MIS, which has a small and confined workspace.

Though this algorithm of tying knots is simple and effective, there are some problems that have been found while conducting experiments. First, it requires end-effectors to rotate for more than 720° during knot-tightening. But actually it is difficult for most end-effectors of the surgical robot systems to rotate for more than 360°. Second, the length of the two threads is significant in this algorithm. Different lengths of the two threads are required for wounds with different sizes. Third, the grasping angle is not arbitrary. It must be along the tangent or the normal to the grasping point. In addition, the image and positioning systems of the robot system should be precise since the grasping angle must change once during knot-tying.

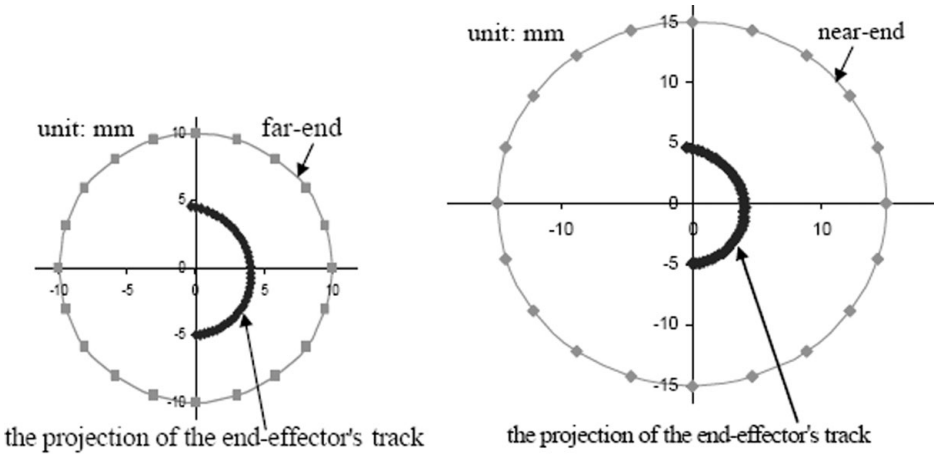

12a. The projection in the far-end 12b. The projection in the near-end

Fig. 12. Simulation of suturing motion in horizontal plane under a laryngoscope tube.

https://doi.org/10.1017/S0263574709990622 Published online by Cambridge University Press

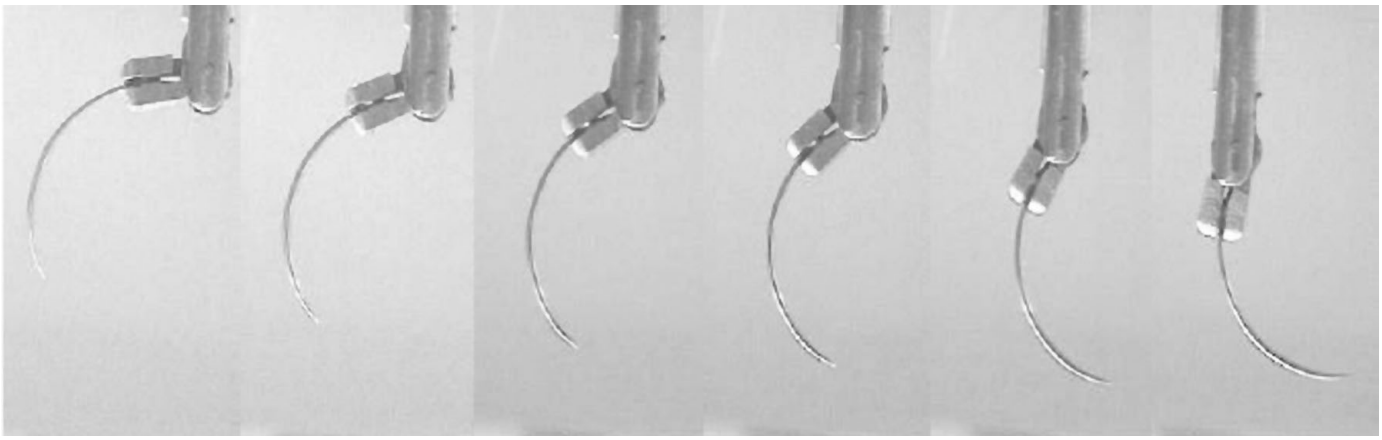

Fig. 13. Experiments on suturing motions in vertical plane.

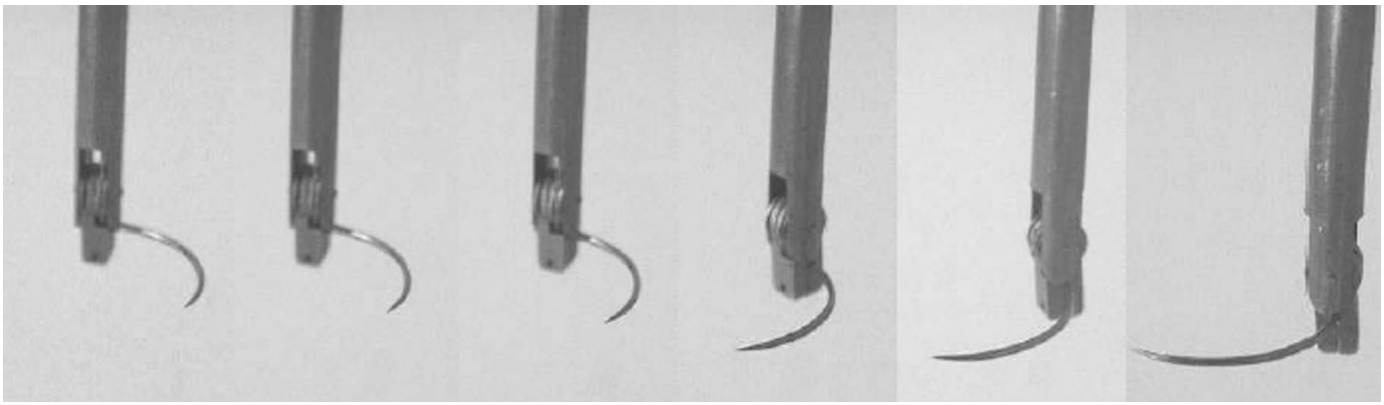

Fig. 14. Experiments on suturing motions in horizontal plane.

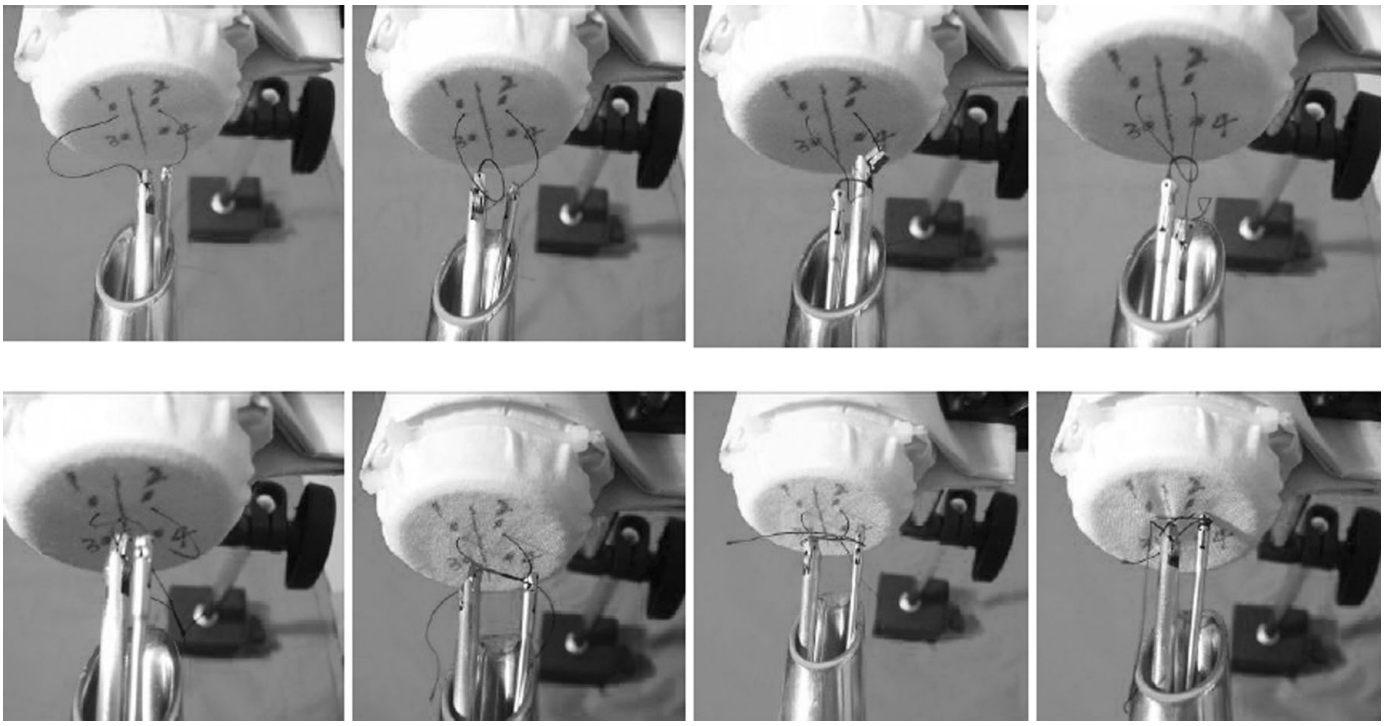

Fig. 15. BTKT experiments assisted by MicroHand III.

https://doi.org/10.1017/S0263574709990622 Published online by Cambridge University Press

7. Conclusions

The operations of suturing and tying knots in laryngeal MIS are assisted by the MicroHand III system with the suturing path planning and the BTKT algorithm. The algorithm can form a stable loop for tying a simple knot. With this algorithm the knot is placed properly and tightened with the specified tension after it is formed in the narrow workspace. MicroHand III is designed for laryngeal surgery with suturing and knot-tying capabilities. The system can facilitate surgeons to accomplish a cooperative motion of multiple end-effectors for complex operations such as suturing and tying knots in a confined workspace.

Acknowledgments

This research was supported by the National High-tech R&D Program of China (863 Program) (Grant No. 2007AA04Z247), the NSFC (Grant No. 50925520), the Tianjin Municipal Science & Technology Development Program (Grant No. 07JCZDJC09000), and the NCET (Program for New Century Excellent Talents in University).

References

1. S. X. Wang, H. J. Wang and L. W. Yue, "A novel knot-tying approach for minimally invasive surgical robot systems," *Int. J. Med. Robotics Computer Assisted Surg.* **4**(3), 268–276 (2008).
2. T. R. Varma, P. R. Eldridge and A. Forster, "Use of the NeuroMate stereotactic robot in a frameless mode for movement disorder surgery," *Stereotactic Funct. Neurosurg.* **80**(1–4), 132–135 (2003).
3. R. H. Taylor, P. Jenson, L. Whitcomb, A. Barnes, R. Kumar, D. Stoianovici, P. Gupta, Z. X. Wang, E. deJuan and L. Kavoussi, "A steady-hand robotic system for microsurgical augmentation," *Int. J. Robotics Res.* **18**, 1201–1210 (1999).
4. R. H. Taylor, B. D. Mittelstadt, H. A. Paul, W. Hanson, P. Kazanzides and J. F. Zuhars, "An image-directed robotic system for precise orthopaedic surgery," *IEEE Transactions on Robotics and Automation* **10**(3), 261–275 (1994).
5. R. H. Taylor and D. Stoianovici, "Medical robotics in computer-integrated surgery," *IEEE Transactions on Robotics and Automation* **19**(5), 765–781 (2003).
6. B. Q. Pei, L. Zhou, K. Lv and T. M. Wang, "The surgery parameters optimizing analysis of the internal fixation of femoral neck fracture," *Chinese J. Biomed. Eng.* **26**(3), 431–440 (2007).
7. K. Cleary, A. Melzer, V. Watson, G. Kronreif and D. Stoianovici, "Interventional robotic systems: Applications and technology state-of-the-art," *Minimally Invasive Ther. Allied Technol.* **15**(2), 101–113 (2006).
8. A. M. Quinn, "CyberKnife®: A robotic radiosurgery system," *Clinical Journal of Oncology Nursing* **6**(3), 149 (2002).
9. A. Hakimi, M. Feder and R. Ghavamian, "Minimally invasive approaches to prostate cancer: A review of the current literature," *Urol. J.* **4**(3), 130–137 (2007).
10. J. P. Ruurda, T. van Vroonhoven and I. Broeders, "Robot-assisted surgical systems: A new era in laparoscopic surgery," *Ann. R. Coll. Surg. Engl.* **84**, 223–226 (2002).
11. M. Meadows, "Computer-assisted surgery: An update," *FDA Consumer Mag.* **39**(4), 16–17 (2005).
12. D. W. Miller, R. T. Schlinkert and D. K. Schlinkert, "Robot-assisted laparoscopic cholecystectomy: Initial Mayo Clinic Scottsdale experience," *Mayo Clin. Proc.* **79**(9), 1132–1136 (2004).
13. J. Heemskerk, R. van Dam, W. G. van Gemert, G. L. Beets, J. W. M. Greve, M. Jacobs and N. D. Bouvy, "First results after introduction of the four-armed da Vinci surgical system in fully robotic laparoscopic cholecystectomy," *Dig. Surg.* **22**(6), 426–431 (2005).
14. N. L. Miller and D. Theodorescu, "Status of robotic cystectomy in 2005," *World J. Urol.* **24**(2), 180–187 (2006).
15. M. Wolfram, R. Braeutigam, T. Engl, W. Bentas, S. Heitkamp, M. Ostwald, W. Kramer, J. Binder, R. Blaheta, D. Jonas and W. D. Beecken, "Robotic-assisted laparoscopic radical prostatectomy: The Frankfurt technique," *World J. Urol.* **21**(3), 128–132 (2003).
16. S. Dogan, T. Aybek, P. Risteski, S. Mierdl, H. Stein, C. Herzog, M. F. Khan, O. Dzemali, A. Moritz and G. Wimmer-Greinecker, "Totally endoscopic coronary artery bypass graft: Initial experience with an additional instrument arm and an advanced camera system," *Surg. Endosc.* **18**(11), 1587–1591 (2004).
17. B. A. Jones, S. Krueger, D. Howell, B. Meinecke and S. Dunn, "Robotic mitral valve repair: A community hospital experience," *Tex. Heart Inst. J.* **32**(2), 143–146 (2005).
18. D. A. Murphy, J. S. Miller, D. A. Langford and A. B. Snyder, "Endoscopic robotic mitral valve surgery," *J. Thorac. Cardiovasc. Surg.* **132**(4), 776–781 (2006).
19. H. Mayer, F. Gomz, D. Wierstra, I. Nagy, A. Knoll and J. Schmidhuber, "A system for robotic heart surgery that learns to tie knots using recurrent neural networks," *Proceedings of the 2006 IEEE/RSJ International Conference on Intelligent Robots and Systems*, Beijing, China (2006).
20. I. K. McLeod and P. C. Melder, "Da Vinci robot-assisted excision of a vallecular cyst: A case report," *Ear, Nose Throat J.* **84**(3), 170–172 (2005).
21. I. K. McLeod, E. A. Mair and P. C. Melder, "Potential applications of the Da Vinci minimally invasive surgical robotic system in otolaryngology," *Ear, Nose Throat J.* **84**(8), 483–487 (2005).
22. N. G. Hockstein, J. P. Nolan, B. W. O'Malley, et al., "Robotic microlaryngeal surgery: A technical feasibility study using the DaVinci surgical robot and an airway mannequin," *Laryngoscope* **115**(5), 780–785 (2005).
23. S. X. Wang, Q. Z. Li, J. N. Ding and Z. J. Zhang, "Kinematic design for robot-assisted laryngeal surgery systems," *2006 IROS IEEE/RSJ International Conference on Intelligent Robots and Systems*, Beijing, China (2006) pp. 2864–2869.
24. A. Kapoor, N. Simaan and R. H. TayJor, "Suturing in confined spaces: Constrained motion control of a hybrid 8-DoF robot," *12th International Conference on Advanced Robotics*, Seattle, US (2005) pp. 452–459.
25. D. K. Pai, "STRANDS: Interactive simulation of thin solids using Cosserat models," *Comput. Graph. Forum* **21**(3), 347–352 (2002).
26. J. Brown, J. C. Latombe and K. Montgomery, "Real-time knot-tying simulation," *Visual Comput.* **20**, 165–179 (2004).
27. J. Phillips, A. Ladd and L. E. Kavraki, "Simulated knot tying," *Proceedings of the 2002 IEEE International Conference on Robotics & Automation*, Washington, DC, Vol. 1 (2002) pp. 841–846.
28. M. Saha and P. Isto, "Motion planning for robotic manipulation of deformable linear objects," *Preceedings of the 2006 IEEE International Conference on Robotics and Automation*, Orlando, FL (2006) pp. 2478–2482.
29. F. Nageotte, M. de Mathelin, C. Doignon, L. Soler, J. Leroy and J. Marescaux, "Computer-aided suturing in laparoscopic surgery," *Int. Congr. Ser.* **1268**, 781–786 (2004).
30. H. Kang and J. T. Wen, "Autonomous suturing using minimally invasive surgical robots," *Proceedings of the 2000 IEEE International Conference on Control Applications*, Anchorage, Alaska (2000) pp. 742–747.
31. J. F. Kuniholm and G. D. Buckner, "Automated knot tying for fixation in minimally invasive," *Robot-Assisted Cardiac Surgery* **127**(11), 1001–1008 (2005).
32. D. L. Murphy, "Endoscopic suturing and knot tying: Theory into practice," *Ann. Surg.* **234**(5), 607–612 (2001).

33. Emin Tuncay Ustuner, "Automatic surgical suturing instrument and method," US Patent 7048748B1 (2006).
34. W. H. Ring, "A new Device for exposure of the oropharynx," *Arch Otolaryngol* **96**(1), 86–87 (1972).
35. J. N. Ding, *Design and Implementation of Laryngeal Minimally Invasive Surgery Robot System with Suturing Ability* (Tianjin University PhD dissertation, 2008).
36. C. G. L. Cao and C. L. MacKenzie, "Task and motion analyses in endoscopic surgery," *1996 ASME IMECE Conference Proceedings: 5th Annual Symposium on Haptic Interfaces for Virtual Environment and Teleoperator Systems*, Atlanta, GA (1996) pp. 583–590.
37. H. Kang and J. T. Wen, "Robotic knot tying in minimally invasive surgeries," *Proceedings of the 2002 IEEE/RSJ International Conference on Intelligent Robots and Systems EPFL*, Lausanne, Switzerland (2002).
38. P. S. Donelan, "Singularity-theoretic methods in robot kinematics," *Robotica* **25**(6), 641–659 (2007).
39. J. S. Dai, "An historical review of the theoretical development of rigid body displacements from Rodrigues parameters to the finite twist," *Mech. Mach. Theory* **41**(1), 41–52 (2006).
40. R. M. Murray, Z. X. Li and S. S. Sastry, *A Mathematical Introduction to Robotic Manipulation* (CRC Press LLC, Boca Raton, FL, 1994).

https://doi.org/10.1017/S0263574709990622 Published online by Cambridge University Press